THE JOURNAL OF PHYSICAL CHEMISTRY C

ARTICLE

pubs.acs.org/JPCC

Surface Defects-Induced p-type Conduction of Silicon Nanowires

Lin-Bao Luo,[†,‡,∥] Xiao-Bao Yang,[†,§,∥] Feng-Xia Liang,[†] Hu Xu,[†] Yu Zhao,[†] Xing Xie,[†] Wen-Feng Zhang,[†] and Shuit-Tong Lee*[,†]

[†]Center of Super-Diamond and Advanced Films (COSDAF) and Department of Physics and Materials Science, City University of Hong Kong, Hong Kong SAR, People's Republic of China

[‡]School of Electronic Science and Applied Physics, Hefei University of Technology, Hefei, Anhui, 230009, People's Republic of China

[§]Department of Physics, South China University of Technology, Guangzhou, 510641, Guangdong Province, People's Republic of China

Supporting Information

ABSTRACT: The fundamental properties of silicon nanowires (SiNWs) are highly dependent on dimension and surface states. Despite many studies of the surface effects on the important properties of SiNWs, the understanding of the interrelation between surfaces and properties remains unclear. Herein we used SiNWs etched from Si wafer as a paradigm to study the relationship of surface states and electrical properties of SiNWs. We showed that, besides hydrogen, SiNW surfaces also consist of adsorbed carbon species, water molecules, and surface defects (P_b center) with a spin density of $C_{spin} = 9.7 \times 10^{12}$ mg^{-1}. Our first-principle calculations revealed that surface defects including P_b, P_{b0}, and P_{b1}, similar to H-defect dangling bonds, can provide acceptor levels to trap electrons, and account for the conversion of transport properties from intrinsic to p-type conduction in SiNWs. We further revealed that SiNW with a diameter of tens to 100 nm would show obvious p-type conduction. Additionally, our theoretical simulation showed that water molecule could increase p-type conduction by lowering the defect energy. Low-temperature $I-V$ measurements showed the defect ionization energy in the p-type SiNW at 36.4 meV.

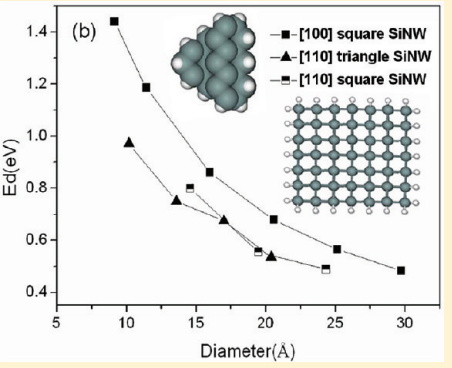

1. INTRODUCTION

Silicon has been central to numerous technological innovations for decades and remains to be the irreplaceable key material for electronic industry.[1−3] Compared with thin film counterparts, nanodevices assembled from silicon nanowires (SiNWs) of several to 100 nm in diameters could achieve enhanced performance and new functions.[4−6] A great deal of effort has been devoted to theoretical simulations of 1D Si nanostructures[7] and their various applications, including field-effect transistors (FETs),[8] lithium ion battery,[9,10] solar cell,[11−13] thermoelectric device,[14,15] photodetectors,[16,17] and surface-enhanced Raman scattering substrates.[18,19]

Owing to the large surface-to-volume ratio, the surface invariably has a strong influence on the total characteristics of Si nanostructures. As a consequence, adsorbents or attached molecules with special function groups will affect the electrical property of SiNWs via changing surface charges, which is the basis of high-sensitivity gas, chemical, and biological detectors.[20] The high surface sensitivity, while beneficial for sensor applications, can lead to difficulty in controllability and reproducibility in devices. Therefore, it is of fundamental and technological importance to understand the relationship of surface and transport properties of SiNWs.[21−24] To date, most studies on this topic are primarily based on either experimental observations with limited understanding of physical origins[25] or theoretical simulations of model systems, which are either too simple or unrealistic.[26,27] In this study, we seek to understand the interconnection between the surface defects and transport properties of SiNWs by combining both experimental investigations and theoretical simulations.

2. EXPERIMENTAL DETAILS

SiNWs were fabricated via silver nanoparticles-assisted chemical method (Supporting Information) developed by our group.[28,29] Scanning electron microscopy (SEM, Philips XL 30 FEG), energy-dispersive X-ray spectroscopy (EDX), and high-resolution transmission electron microscopy (HRTEM, CM200 FEG, operating at 200 KV) were used to study the morphology, crystal structure, and chemical composition of SiNWs. X-ray photoelectron spectroscopy (XPS) was performed on a VG ESCALAB 3 spectrometer, using a monochromatic Al Kα source (1486.6 eV) at a base pressure of $<10^{-9}$ Torr. For ESR measurements, ∼20 mg of SiNWs powder was filled into a standard ESR quartz sample tube. The ESR system (Bruker EMX-10/12) was operated at 9.75 GHz, with microwave modulation frequency of 100 kHz and modulation amplitude of 0.2 G. For quantitative analysis, emery stone (g = 2.005) with a spin density of 10^{15} was employed as reference standard. SiNW FET devices were fabricated (Supporting Information) and used to

Received: June 2, 2011
Revised: August 8, 2011
Published: August 19, 2011

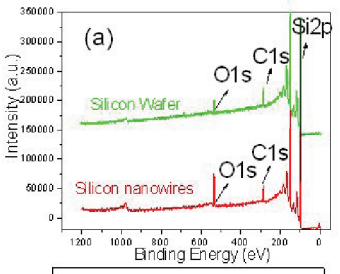

(b)	Si (%)	O (%)	C (%)
Si wafer	84.73	3.63	11.65
SiNWs	78.23	10.25	11.51

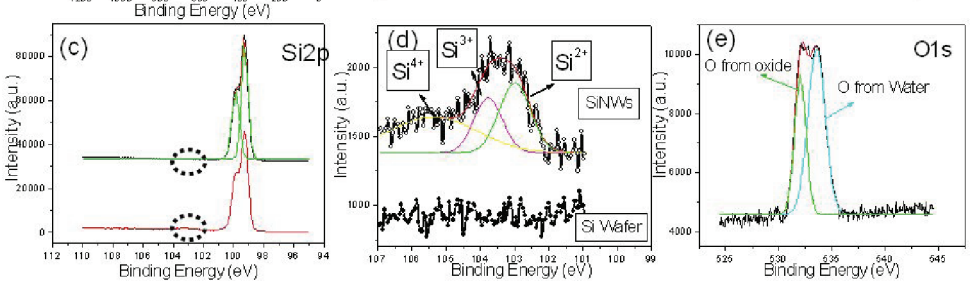

Figure 1. Typical XPS spectra of Si wafer and SiNWs after brief immersion in diluted HF solution. (a) Survey spectra of Si wafer and SiNWs. (b) Chemical composition of Si wafer and SiNWs. (c) XPS spectra for Si2p peak. (d) Si2p spectra for SiNWs and Si wafer at higher resolution. (e) O1s spectrum for SiNWs at higher resolution.

study the transport properties and defect ionization energy of SiNWs. The temperature-dependent electrical studies were performed in the range of 300 to 85 K by using a home-built setup equipped with an $I-V$ measurement system (Keithley 4200-SCS, semiconductor characterization system) with automatic cooling (Perfect lab).

3. RESULTS AND DISCUSSION

The reason for using silver-catalyzed etching rather than another method (e.g., vapor−liquid−solid (VLS) or oxide-assisted growth method (OAG)) to prepare SiNWs is based on the following advantages of the etched SiNWs: (1) Both the length and diameter of SiNWs can be readily tuned by adjusting silver nanoparticles catalysts and etching duration.[30] Such dimension control is helpful to fabrication of FET devices. (2) The core of SiNWs maintains the crystalline structure and inherits the well-defined electrical properties of the mother wafer. This feature enables direct comparison of the transport properties of SiNWs and the mother wafer, which facilitates the study of surface state effects on transport properties.[31]

Similar to SiNWs obtained from OAG method,[32,33] the surfaces of etched SiNWs after brief HF immersion are also H-terminated.[24] The chemical composition of the etched SiNWs was investigated by XPS. As shown in the Figure 1a, the XPS spectra of both Si wafer and SiNWs consist of three peaks at 99, 285, and 532.5 eV due to Si, C, and O, respectively. The determined atomic ratio is shown in Figure 1b. The carbon peak due to surface contamination is invariably present in the XPS spectrum of semiconductor nanostructures, and its nominal influence can be left aside in this study.[34,35] The higher intensity of the O peak from SiNWs than Si wafer is due to the large surface-to-volume ratio of SiNWs (Figure 1 of the Supporting Information). The Si peak was scanned for higher spectral intensity and resolution. Figure 1c depicts the Si 2p spectra obtained on SiNWs and Si wafer. Both spectra consist of two peaks at 99.3 and 99.86 eV, due to $2p_{1/2}$ and $2p_{3/2}$ states respectively.[36] However, the XPS spectrum of SiNWs shows a weak, broad, and asymmetrical peak in the range of 101−107 eV, which is not present in that of Si substrate. Such a peak can be deconvoluted into three separate ones located at 103.0, 103.9, and 105.3 eV, which can readily be assigned to the Si2p for Si(II), Si(III), and Si(IV) bonded to a different number of oxygen atoms, respectively.[37,38] Note that the 10% oxygen content derived from the XPS of SiNWs is substantially higher than the oxygen bonded to Si as surface silicon oxide or suboxide, which is typically <5%, so the excess oxygen is attributed to the adsorbed H_2O. Furthermore, the presence of water molecules was also confirmed by the corresponding O1s study. As shown in Figure 1e, the O1s spectrum can be deconvoluted into two peaks, one of which is due to oxygen from the oxide and the other from water molecules.

Point defects are expected to exist in SiNWs due to the rough surface and the presence of oxygen. We performed ESR measurements to investigate the defects in the as-etched SiNWs (Figure 2a). The ESR spectra measured at 5 mW and above show a strong resonance at a magnetic field of 3474.8 G with a line width of 12 G and a corresponding g factor of 2.00518.[39] According to the literature, such an electron spin resonance defect is commonly referred to as the P_b center, which arises from the inherent mismatch between Si and SiO_2 lattices.[40] This defect, or more precisely nonbonded dangling bond, may exist in slightly different forms, depending on Si interface orientations. Previous works established that there is only one defect form on both (111) and (110) Si wafers, which is designated as $\bullet Si{\equiv}Si_3$. However, there are two types of P_b centers on the (100) Si wafer: P_{b0} and P_{b1}.[41] Because the SiNWs used in this study is relatively rough (Figure 2 of the Supporting Information), exposing many of the crystallographic facets, consequently any form of P_b centers discussed above may exist on the SiNWs surface (Figure 2c). Although it is impossible to determine accurately the individual percentage, the overall spin density of P_b centers (C_{spin}) can be calculated from the ESR line by double integration of the experimental curve and by comparison with the ESR line of emery stone (Figure 2b). For the etched SiNWs, an overall spin concentration of $C_{spin} = 9.7 \times 10^{12}$ mg^{-1} was obtained, which is nearly 1/66 of $C_{spin} = 6.5 \times 10^{14}$ mg^{-1} in SiNWs fabricated via

dx.doi.org/10.1021/jp205171j |J. Phys. Chem. C 2011, 115, 18453–18458

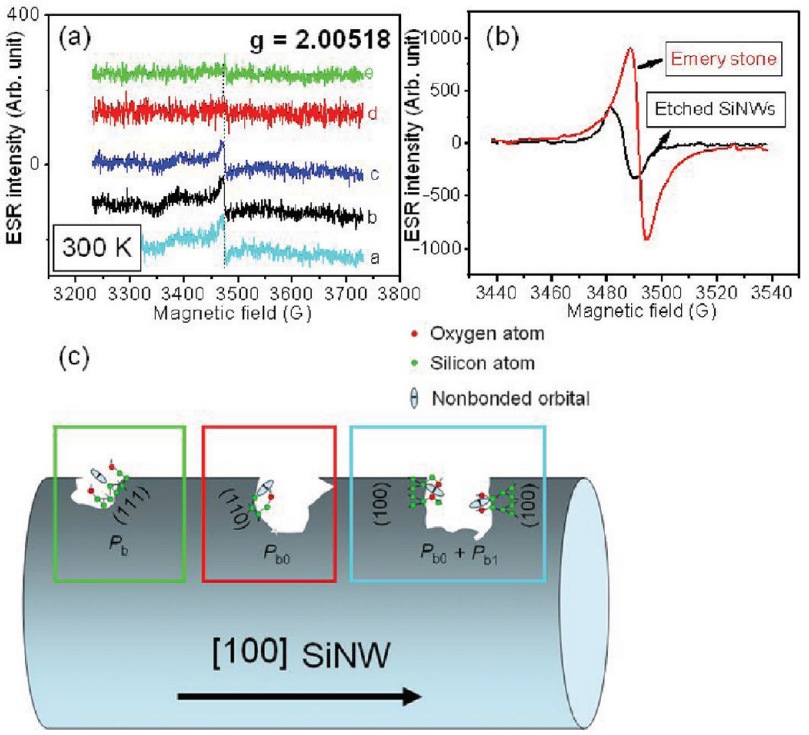

Figure 2. (a) Room-temperature ESR spectra of SiNWs powder obtained at different powers: (a) 20, (b) 10, (c) 5, (d) 1, and (e) 0.2 mW. (b) ESR spectra of both etched SiNWs and emery stone. (c) Schematical illustration of different kinds of P_b centers on SiNWs surface.

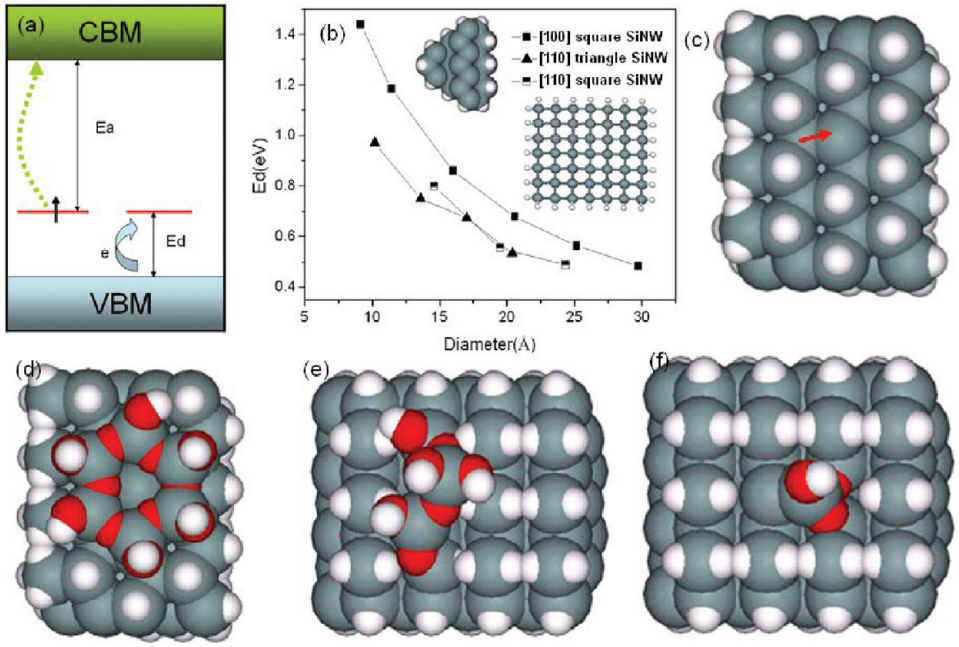

Figure 3. (a) Schematic illustration of electronic structure of SiNWs with an H-defect dangling bond. (b) Defect level energy for SiNWs with different growth orientations and cross sections. Inset are top views of [110] SiNW with a triangle cross section (upper) and [100] SiNW with a square cross section (lower). (c–f) Defects on [110] oriented SiNW facets. Side views of (c) H-defect dangling bond, (d) P_b-center on (111) facet, (e) P_{b0} on (100) facet, and (f) P_{b1} on (100) facet.

OAG method.[42] Such a difference in spin density may result from different synthetic mechanisms.

Recent theoretical studies showed that surface dangling bonds (SDBs) behaved as charge trap centers and could asymmetrically deactivate n- or p-type doping in Si and Ge nanostructures.[43,44] Comparison of the defect levels of SDBs and Au impurities in the Si shell suggested that SDB defects are responsible for the hole concentration in Ge/Si core–shell nanowires.[43] We similarly

dx.doi.org/10.1021/jp205171j |J. Phys. Chem. C 2011, 115, 18453–18458

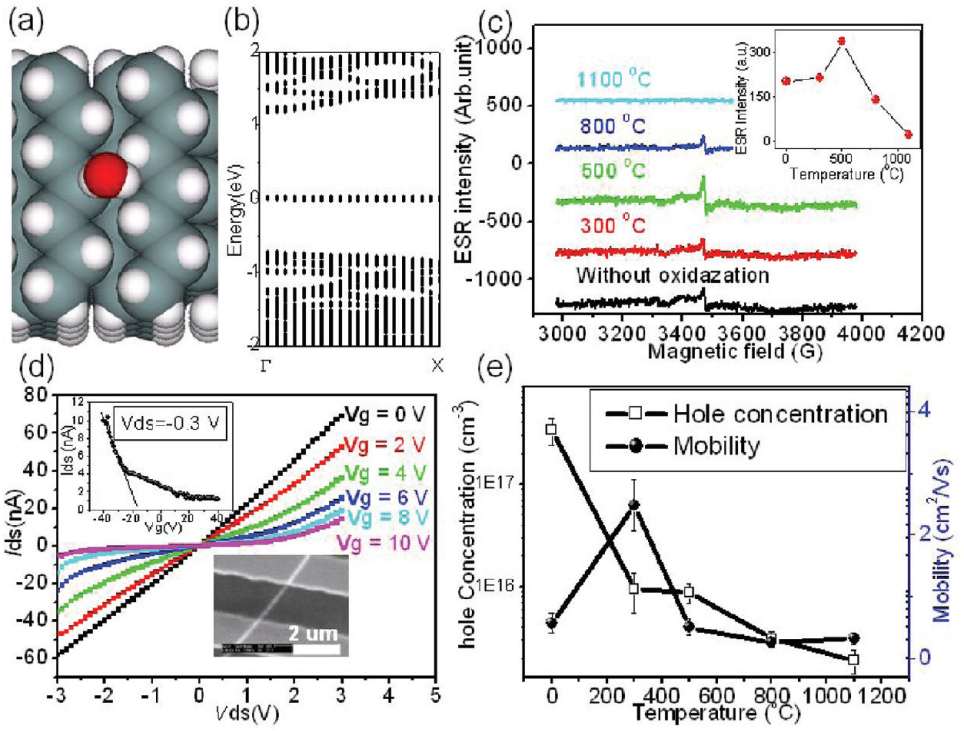

Figure 4. (a) Geometry of SiNW with an adsorbed water molecule. (b) Band structure for part a. (c) ESR spectra of SiNWs thermally oxidized at different temperatures for 1 h; inset is corresponding ESR intensity versus thermal treatment temperature. (d) $I_{ds}-V_{ds}$ plots of SiNW at different V_g. The insets show a logarithmic plot of the transfer characteristics at $V_{ds}= -0.3$ V (upper) and an SEM image of a single-SiNW FET (lower). (e) Carrier concentration and mobility of the SiNW versus oxidation temperature.

examined the influence of P_b centers on the electronic structure of the etched SiNWs by density functional theory (DFT) calculation (Supporting Information) to investigate defect-induced conductivity and physics of SiNWs surfaces etched from Si wafer. Because of the diversity of P_b centers, it is difficult to accommodate all possible surface defects on a small-diameter SiNW surface. Therefore, the surface defect was substituted with hydrogen-defect dangling bond, formed by removing hydrogen atom from the hydrogen-terminated SiNW surface. This simplification is justified by the structural similarity between the H-defect dangling bond and P_b, P_{b0}, and P_{b1}. The defect level comparison in the following paragraph indeed supports this practice. Simulation results showed that the defect level (E_d) in a square [100] SiNW with a diameter of 16 Å is 0.86 eV above the valence band maximum (VBM) and 1.13 eV (E_a) below the conduction band minimum (CBM). The defect energies imply that it is easier for electrons to be drawn from VBM than to be released into CBM, and thus dangling bonds would produce holes and render SiNWs p-type conducting. Furthermore, defect levels in [100] square, [110] square, and triangle SiNWs are observed to decrease with increasing diameter (Figure 3b). Understandably, as SiNW diameter increases, the defect level will move increasingly closer to the VBM, whereas the band gap will approach the bulk value of 1.1 eV. Consequently, $E_d \ll E_a$ is expected for SiNW with a diameter of tens to 100 nm, which will thus show obvious p-type electrical conduction.

Next, we examined SiNW with different kinds of defects including H-defect dangling bond, P_b, P_{b0}, and P_{b1}. For straightforward comparison, the SiNWs were all [110] oriented and enclosed by (111) and (100) facets (Figure 3c–f). The E_d/E_a are calculated to be 0.95/1.30, 0.88/1.04, 1.11/1.27, and 0.89/1.23 eV for H-defect dangling bond, P_b, P_{bo}, and P_{b1}, respectively. Because E_d/E_a is <1, energy consideration thus suggests that all forms of P_b centers would lead to p-type conduction characteristics. Furthermore, when the diameter of SiNW increased from 0.95 to 1.59 nm, the defect level decreased from 0.97 to 0.65 eV for H-defect dangling bond and from 0.88 to 0.64 eV for P_b center, suggesting that for SiNWs with a larger diameter, the influence of P_b center and H-defect on conductivity is comparable. The theoretical analysis indeed showed that surface defects (P_b center) induced p-type doping of etched SiNWs. The theoretical results are also in agreement with our previous experimental observations that intrinsic SiNW with only P_b centers showed obvious p-type conduction behavior in vacuum.[24]

Because water molecules readily adsorb on the SiNWs surface we also considered their influence on the electrical property of SiNW. Figure 4a depicts a typical SiNW with an H-defect dangling bond and an adsorbed water molecule: One H atom of H_2O points directly at the H-defect dangling bond, and the distance between the Si (with the dangling bond) and H atom is 2.67 Å. E_d is at 0.76 eV for adsorbed water, which is 0.12 eV smaller than that without H_2O adsorption. Apparently, this decrease in defect energy due to water adsorption on surface defect would lead to increased p-type conductivity. This observation is totally different from the case when NH_3 molecule absorbed on the dangling bond, which induced n-type conduction behavior.[45] Note that the defect energy variation due to adsorbed H_2O is highly dependent on the distance between the surface defect and H_2O, with the defect energy decreasing less with increasing distance (results not shown).

dx.doi.org/10.1021/jp205171j |J. Phys. Chem. C 2011, 115, 18453–18458

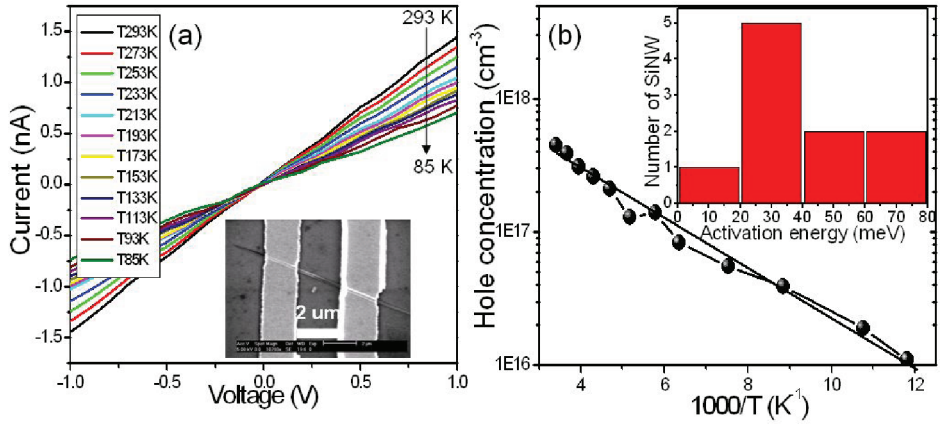

Figure 5. $I-V$ curves of SiNWs measured at a series of temperature: 293, 273, 253, 233, 213, 193, 173, 153, 133, 113, 93, and 85 K; inset is a typical SEM image of the SiNW FET. (b) Temperature dependence of hole concentration on reciprocal temperature. Inset is the distribution of the ionization energy for 10 SiNWs.

We investigated the enhancement effect of p-type conduction by adsorbed water molecules by analyzing the transport properties of SiNWs after thermal treatment. Figure 3 of the Supporting Information plots the oxygen content versus thermal treatment. Basically, the oxygen content increased with increasing temperature from 300 to 1200 °C. The corresponding ESR analysis revealed that spin density increased at first when SiNWs were oxidized at 300 and 500 °C but began to decrease at higher temperatures. The origin of the defect variation is unclear. Transport study showed that the SiNW without thermal treatment showed obvious p-type conduction behavior.[46] The hole concentration and mobility were calculated to be 1.35×10^{17} cm^{-3} and 4.18 cm/V^{-1}s^{-1}, respectively. (See Supporting Information.) After SiNW was oxidized at 300, 500, 800, and 1100 °C, its hole concentration decreased, respectively, to $(9.54, 8.8, 3.1, \text{and } 1.9) \times 10^{15}$ cm^{-3}. The decrease in carrier concentration is understandable considering the weakened influence of the adsorbed H_2O. Because of water adsorption on P_b centers, the hole concentration of the etched SiNW without thermal treatment contains the contribution from both P_b center and water molecule. Upon thermal treatment of SiNW, although the density of P_b center increased a little bit, which would increase hole concentration, the formation of a thin Si dioxide layer failed to lower the defect level due to increase in distance between the silicon core and water molecule, which therefore caused reduced hole concentration. (For more information on the defect level of SiNWs with a water molecule on P_b center, please refer to the Supporting Information.) However, the mobility variation in SiNWs remains unclear and needs further investigation.[47]

The above analysis shows that surface defects indeed form an acceptor level that lies above the valence band and traps electrons. It suggests that the holes generated within SiNWs are due to thermal activation of the defects. The defects can be further verified by temperature-dependent $I-V$ measurements. Figure 5a shows that the electrical conduction of an individual SiNW decreases with decreasing temperature, consistent with defects-induced conductivity.

Another evidence of the thermal activation mechanism rather than electron-drawing mechanism for p-type conduction is the low energy required to supply the hole from the shallow acceptor level ($E_{acceptor}$) into valence band ($E_{valence}$), which is commonly referred to as defect ionization energy or activation energy (E_i) in semiconductors. Because etched SiNWs exhibit p-type conduction, the temperature dependency of hole concentration is given by

$$p = \left(\frac{N_a N_v}{g_d}\right)^{1/2} \exp\left(\frac{-E_i}{k_b T}\right) \quad (1)$$

where N_a is the concentration of acceptors formed by P_b centers, N_v is the effective density of states for the valence band, g_d is the degeneracy factor, T is temperature, and k_b is the Boltzmann constant (1.38×10^{-23} J K^{-1}).

Taking the logarithm yields

$$\lg p = \frac{1}{2}\lg\left(\frac{N_a N_v}{g_d}\right) + \left(\frac{-E_i}{k_b \times 1000 \times 2.3}\right) \times \frac{1000}{T} \quad (2)$$

To extract the ionization energy of the acceptor in the wire, we plotted lg p versus the reciprocal T. Figure 5 shows that fitting the curve into a linear line yields a slope of −0.184. As the slope is equal to $E_i/k_b \times 1000 \times 2.3$, E_i is calculated to be 36.4 meV.[48,49] Measurements of over 10 SiNWs (inset of Figure 5b) showed that the majority of activation energies lie in the range of 20−60 meV. Such activation energy is close to the impurity ionization energy of silicon doped with boron (0.045 eV) or aluminum (0.06 eV). The defect ionization energy is comparable to the thermal energy k_bT (0.026 eV), suggesting that even at room temperature the acceptor level due to surface defects (P_b center) can provide a very high hole concentration via thermal activation mechanism.[47]

To summarize, we have systematically studied the surface states and electronic structure of SiNWs fabricated by the chemical etching method. In addition to hydrogen, the etched SiNW surface consisted of adsorbed water molecules and surface defects (P_b center), as revealed by XPS and ESR measurements. The g value for the P_b center is at 2.00518, and the spin concentration is $C_{spin} = 9.7 \times 10^{12}$ mg^{-1}. DFT calculations showed that H-defect dangling bonds and surface defects of P_b, P_{b0}, and P_{b1} could induce p-type doping of SiNW by trapping electrons, and SiNWs with tens to 100 nm diameters would exhibit p-type conductivity. Calculation showed that water adsorbed on surface defects can also enhance p-type conduction. Low-temperature $I-V$ measurement revealed defect ionization energy of SiNW at 36.4 meV. The totality of our data confirmed

dx.doi.org/10.1021/jp205171j |J. Phys. Chem. C 2011, 115, 18453–18458

the dominant role that surface defects (P_b centers) played in determining the electrical properties of SiNWs.

■ ASSOCIATED CONTENT

Supporting Information. Synthesis and characterization of SiNWs, fabrication of SiNW FET, description of theoretical calculation, BET measurement, EDX analysis of the SiNWs after thermal oxidization, calculation of mobility, and hole concentration of SiNWs. This material is available free of charge via the Internet at http://pubs.acs.org.

■ AUTHOR INFORMATION

Corresponding Author
*E-mail: appannale@cityu.edu.hk,.

Notes
‖Co-first author.

■ ACKNOWLEDGMENT

The work was supported by the Research Grants Council of Hong Kong SAR, China CRF grant (no. CityU5/CRF/08), RGC/NSFC Joint Research grant (no. N_CityU 108/08) and NSFC (No. 21101051).

■ REFERENCES

(1) Sze, S. M. *Physics of Semiconductor Devices*; John Wiley & Sons: New York, 1981.
(2) Cui, Y.; Lieber, C. M. *Science* **2001**, *291*, 851–853.
(3) Teo, B. K.; Sun, X. H. *Chem. Rev.* **2007**, *107*, 1454–1532.
(4) Baca, A. J.; Ahn, J. H.; Sun, Y. G.; Meitl, M. A.; Menard, E.; Kim, H. S.; Choi, W. M.; Kim, D. H.; Huang, Y.; Rogers, J. A. *Angew. Chem., Int. Ed.* **2008**, *47*, 5524–5542.
(5) Schmidt, V.; Wittermann, J. V.; Goesele, U. *Chem. Rev.* **2010**, *110*, 361–388.
(6) Ma, D. D. D.; Lee, C. S.; Au, F. C. K.; Tong, S. Y.; Lee, S. T. *Science* **2003**, *299*, 1874–1877.
(7) Hong, K. H.; Kim, J. S.; Lee, J. H.; Shin, J. W.; Chung, U. I. *Nano Lett.* **2010**, *10*, 1671–1676.
(8) Huang, Y.; Duan, X. F.; Cui, Y.; Lauhon, L. J.; Kim, K. H.; Lieber, C. M. *Science* **2001**, *294*, 1313–1317.
(9) Chan, C. K.; Peng, H. L.; Liu, G.; Mcllwrath, K.; Zhang, X. F.; Huggins, R. A.; Cui, Y. *Nat. Nanotechnol.* **2008**, *3*, 31–35.
(10) Magasinski, A.; Dixon, P.; Hertzberg, B.; Kvit, A.; Ayala, J.; Yushin, G. *Nat. Mater.* **2010**, *9*, 353–358.
(11) Tian, B. Z.; Zheng, X. L.; Kempa, T. J.; Fang, Y.; Yu, N. F.; Yu, G. H.; Huang, J. L.; Lieber, C. M. *Nature* **2007**, *449*, 885–890.
(12) Peng, K. Q.; Wang, X.; Wu, X. L.; Lee, S. T. *Nano Lett.* **2009**, *9*, 3704–3709.
(13) Goodey, A. P.; Eichfeld, S. M.; Lew, K. K.; Redwing, J. M.; Mallouk, T. E. *J. Am. Chem. Soc.* **2007**, *129*, 12344–12345.
(14) Hochbaum, A. I.; Che, R. K.; Delgado, R. D.; Liang, W. J.; Garnett, E. C.; Najarian, M.; Majumdar, A.; Yang, P. D. *Nature* **2008**, *451*, 163–168.
(15) Boukai, A. I.; Bunimovich, Y.; Tahir-Khell, J.; Yu, J. K.; Goddard, W. A.; Heath, J. R. *Nature* **2008**, *451*, 168–171.
(16) Yang, C.; Barrelet, C. J.; Capasso, F.; Lieber, C. M. *Nano Lett.* **2006**, *6*, 2929–2934.
(17) Zhang, A.; Kim, H. K.; Cheng, J.; Lo, Y. H. *Nano Lett.* **2010**, *10*, 2117–2120.
(18) Zhang, M. L.; Yi, C. Q.; Fan, X.; Peng, K. Q.; Wong, N. B.; Yang, M. S.; Zhang, R. Q.; Lee, S. T. *Appl. Phys. Lett.* **2008**, *92*, 043116.
(19) Qiu, T.; Wu, X. L.; Shen, J. C.; Ha, P. C. T.; Chu, P. K. *Nanotechnology* **2006**, *17*, 5769–5772.
(20) Patolsky, F.; Zheng, G. F.; Lieber, C. M. *Nat. Protoc.* **2006**, *1*, 1711–1724.
(21) Cui, Y.; Zhong, Z. H.; Wang, D. L.; Wang, W. U.; Lieber, C. M. *Nano Lett.* **2003**, *3*, 149–152.
(22) Haick, H.; Hurley, P. T.; Hochbaum, A. I.; Yang, P. D.; Levis, N. S. *J. Am. Chem. Soc.* **2006**, *128*, 8990–8991.
(23) Jie, J. S.; Zhang, W. J.; Peng, K. Q.; Yuan, G. D.; Lee, C. S.; Lee, S. T. *Adv. Funct. Mater.* **2008**, *18*, 3251–3257.
(24) Guo, C. S.; Luo, L. B.; Yuan, G. D.; Yang, X. B.; Zhang, R. Q.; Zhang, W. J.; Lee, S. T. *Angew. Chem., Int. Ed.* **2009**, *48*, 9896–9990.
(25) Zhou, X. T.; Hu, J. Q.; Li, C. P.; Ma, D. D. D.; Lee, C. S.; Lee, S. T. *Chem. Phys. Lett.* **2003**, *369*, 220–224.
(26) Lu, A. J.; Zhang, R. Q. *Solid State Commun.* **2008**, *145*, 275–278.
(27) Qi, W. H.; Lee, S. T. *Chem. Phys. Lett.* **2009**, *483*, 247–249.
(28) Zhang, M. L.; Peng, K. Q.; Fan, X.; Jie, J. S.; Zhang, R. Q.; Lee, S. T.; Wong, N. B. *J. Phys. Chem. C* **2008**, *112*, 4444–4450.
(29) Luo, L. B.; Jie, J. S.; Zhang, W. F.; He, Z. B.; Wang, J. X.; Yuan, G. D.; Zhang, W. J.; Wu, L. C. M; Lee, S. T. *Appl. Phys. Lett.* **2009**, *94*, 193101.
(30) Huang, Z. P.; Fang, H.; Zhu, J. *Adv. Mater.* **2007**, *19*, 744 –750.
(31) Cui, Y.; Duan, X. F.; Hu, J. T.; Lieber, C. M. *J. Phys. Chem. B* **2000**, *104*, 5213–5216.
(32) Sun, X. H.; Wang, S. D.; Wong, N. B.; Ma, D. D. D.; Lee, S. T. *Inorg. Chem.* **2003**, *42*, 2398–2404.
(33) Chen, W. W.; Sun, X. H.; Wang, S. D.; Lee, S. T.; Teo, B. K. *J. Phys. Chem. C* **2005**, *21*, 10871–10879.
(34) Xiang, B.; Wang, P. W.; Zhang, X. Z.; Dayeh, S.; Aplin, D. P. R.; Soci, C.; Yu, D. P.; Wang, D. R. *Nano Lett.* **2007**, *7*, 323–328.
(35) Song, H. S.; Zhang, W. J.; Yuan, G. D.; He, Z. B.; Zhang, W. F.; Tang, Y. B.; Luo, L. B.; Lee, C. S.; Bello, I.; Lee, S. T. *Appl. Phys. Lett.* **2009**, *95*, 033117.
(36) Barrett, N. T.; Renault, O.; Damlencourt, J. F.; Martin, M. J. *J. Appl. Phys.* **2004**, *96*, 6362–6369.
(37) Cerofolini, G. F.; Galati, C.; Renna, L. *Surf. Interface Anal.* **2003**, *35*, 968–973.
(38) Nucho, R. N.; Madhukar, A. *Phys. Rev. B* **1980**, *21*, 1576–1588.
(39) Wertz, J. E.; Bolton, J. R. *Electron Spin Resonance: Elementary Theory and Practical Application*; Chapman and Hall: New York, 1986.
(40) Poindexter, E. H.; Caplan, P. J. *J. Appl. Phys.* **1981**, *52*, 879–884.
(41) Poindexter, E. H.; Caplan, P. J. *J. Vac. Sci. Technol., A* **1988**, *6*, 1352–1357.
(42) Baumer, A.; Stutzmann, M.; Brandt, M. S.; Au, F. C. K.; Lee, S. T. *Appl. Phys. Lett.* **2004**, *85*, 943–945.
(43) Park, J.; Ryu, B.; Moon, C.; Chang, K. J. *Nano Lett.* **2010**, *10*, 116–121.
(44) Hong, K.; Kim, J.; Lee, J. H.; Shin, J.; Chung, U. *Nano Lett.* **2010**, *10*, 1671–1676.
(45) Miranda-Duran, A.; Cartoixa, X.; Irisson, M. C.; Rurali, R. *Nano Lett.* **2010**, *10*, 3590–3595.
(46) Yuan, G. D.; Zhou, Y. B.; Guo, C. S.; Zhang, W. J.; Tang, Y. B.; Li, Y. Q.; Chen, Z. H.; He, Z. B.; Zhang, X. J.; Wang, P. F.; Bello, I.; Zhang, R. Q.; Lee, C. S.; Lee, S. T. *ACS Nano* **2010**, *4*, 3045–3052.
(47) Schmidt, V.; Wittemann, J. V.; Senz, S.; Gosele, U. *Adv. Mater.* **2009**, *21*, 2681–2702.
(48) Neamen, D. A. *Semiconductor Physics and Devices: Basic Principles*, 3rd ed.; McGraw-Hill: Boston, 2003.
(49) Bjork, M. T.; Schmid, H.; Hnoch, J.; Riel, H.; Riess, W. *Nat. Nanotechnol.* **2009**, *4*, 103–107.